HHS Public Access

Author manuscript

J Am Chem Soc. Author manuscript; available in PMC 2020 May 08.

Published in final edited form as:

J Am Chem Soc. 2019 June 19; 141(24): 9479–9484. doi:10.1021/jacs.9b03157.

A Terminal Fe^{III}-Oxo in a Tetranuclear Cluster: Effects of Distal Metal Centers on Structure and Reactivity

Christopher J. Reed, **Theodor Agapie***

Division of Chemistry and Chemical Engineering, California Institute of Technology, Pasadena, California 91125, United States

Abstract

Tetranuclear Fe clusters have been synthesized bearing a terminal Fe^{III}-oxo center stabilized by hydrogen bonding interactions from pendant *tert*-butyl amino pyrazolate ligands. This motif was supported in multiple Fe oxidation states, ranging from $[Fe^{II}_2Fe^{III}_2]$ to $[Fe^{III}_4]$; two oxidation states were structurally characterized by single crystal X-ray diffraction. The reactivity of the Fe^{III}-oxo center in proton coupled electron transfer (PCET) with X–H (X = C, O) bonds of various strengths was studied in conjunction with analysis of thermodynamic square schemes of the cluster oxidation states. These results demonstrate the important role adjacent metal centers have on modulating the reactivity of a terminal metal-oxo.

Graphical Abstract

Authors are required to submit a graphic entry for the Table of Contents (TOC) that, in conjunction with the manuscript title, should give the reader a representative idea of one of the following: A key structure, reaction, equation, concept, or theorem, etc., that is discussed in the manuscript. Consult the journal's Instructions for Authors for TOC graphic specifications.

*Corresponding Author: agapie@caltech.edu.

Supporting Information

The Supporting Information is available free of charge on the ACS Publications website.

Experimental Procedures and Supplimentary Data (PDF)

Crystallographic data files (CIFs)

The authors declare no competing financial interests.

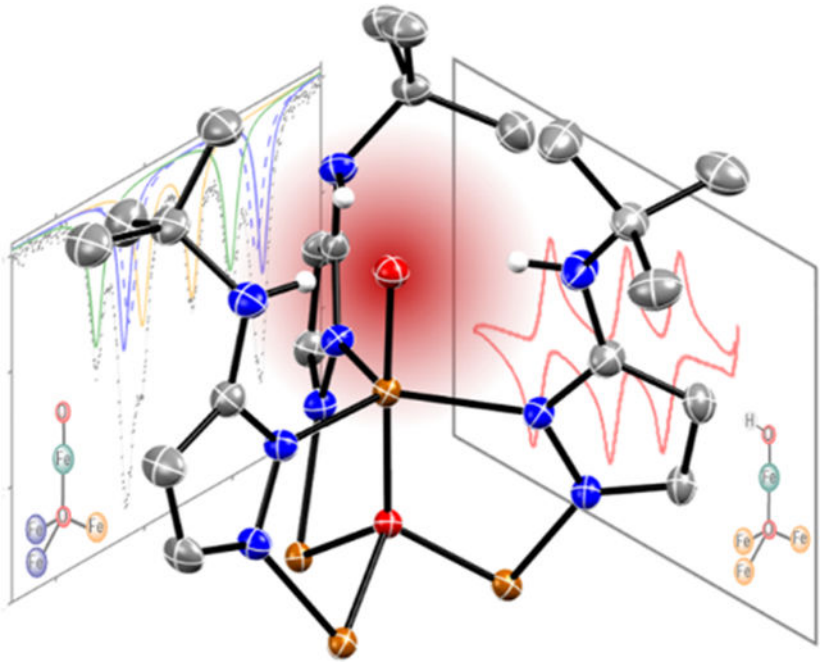

Terminal metal-oxo moieties are invoked as key intermediates in both natural and synthetic catalysts of mid-first-row transition metal ions (Mn, Fe, and Co).[1] For example in photosynthesis, water is oxidized in photosystem II by a $CaMn_4O_5$ cluster known as the oxygen evolving complex (OEC);[2] numerous computational studies of the catalytic mechanism have proposed a high-valent Mn-oxo playing a key role in O–O bond formation.[3] Similarly, a number of synthetic water oxidation catalysts employing various multinuclear scaffolds have been reported, where a terminal metal-oxo is implicated as a key intermediate (Figure 1).[1e–g, 4]

Studies of synthetic transition metal-oxo complexes have been integral for understanding these reactive moieties in catalytic systems.[1a, 5] However, there is a paucity of literature concerning multinuclear complexes bearing well-characterized terminal metal-oxo motifs.[6] In a rare example where the effects of a neighboring metal oxidation state on a terminal metal-oxo could be interrogated, Que and coworkers reported that the spin state of an Fe^{IV}-oxo center would change depending on the oxidation state of a neighboring Fe in a μ_2-O bridged bimetallic complex ($L'_2OFe_2(OH)(O)^{2+/3+}$).[6c] The authors demonstrated that structural and spin-state changes due to reduction of this secondary Fe leads to a thousand-fold activation of the [Fe_2] complex towards C–H oxidation.

To gain further insights into these multimetallic effects, our group has examined well-defined tetranuclear clusters of Fe and Mn, which facilitate intramolecular oxygen atom transfer reactions; however, a terminal metal-oxo intermediate could not be observed.[7] Inspired by reports of mononuclear terminal metal-oxo motifs stabilized by second coordination sphere hydrogen bonding interactions,[8] our group has previously used this strategy to access a terminal Mn^{III}–OH moiety as part of a [Mn_4] cluster.[9] Herein, we describe the synthesis, structural characterization, and reactivity studies of clusters bearing a

terminal Fe^{III}-oxo motif, stabilized by *tert*-butyl-amino-pyrazolates, to probe the significance of a multinuclear scaffold on structural and reactivity aspects of a terminal metal-oxo.

Treating the reported **$LFe_3(OAc)(OTf)_2$** cluster ($^{-}$OTf, triflate = trifluoromethane sulfonate)[10] with three equivalents of potassium *tert*-butyl-amino-pyrazolate (KPzNHtBu) and iodosylbenzene (PhIO), followed by addition of iron (II) triflate bis-acetonitrile ($Fe(OTf)_2$ • 2 MeCN) and excess potassium hydroxide in tetrahydrofuran produces the neutral [$Fe^{II}_3Fe^{III}$] cluster, **1** (Scheme 1). Single crystal X-ray diffraction (XRD) studies of **1** reveal a structure similar to our previously reported [Mn_4] cluster bearing a terminal hydroxide ligand (Figure 2A);[9] the apical metal displays a trigonal bipyramidal geometry, with the terminal hydroxide ligand hydrogen bonded to each amino-pyrazolate (N–O distances of 2.826(1), 2.765(1), 2.789(1) Å for **1**). The relatively short distance between the apical Fe and the interstitial μ_4-O (Fe4–O1), 1.837(1) Å, is consistent with an Fe^{III} in the apical position of the cluster, with the remaining Fe centers being Fe^{II}.[7b, 11]

The electrochemistry of the [Fe_4] hydroxide clusters in THF features three quasi-reversible events assigned to the [$Fe^{II}_3Fe^{III}$]→[$Fe^{II}_2Fe^{III}_2$] (−1.53 V; all potentials vs. Fc/Fc^{+}), [$Fe^{II}_2Fe^{III}_2$]→[$Fe^{II}Fe^{III}_3$] (−0.68 V), and [$Fe^{II}Fe^{III}_3$]→[Fe^{III}_4] (−0.10 V) redox couples (Figure S36). Each of the corresponding oxidation states of the cluster could be isolated (Scheme 1). Mössbauer spectra of the oxidized clusters **2**, **3**, and **4** are consistent with oxidations occurring at the Fe^{II} centers in the tri-iron core and the Fe–OH moiety remaining Fe^{III} (Figures 2C, S42, S46, and S47).

Access to a terminal Fe^{III}-oxo moiety was achieved by deprotonation of the [$Fe^{II}_2Fe^{III}_2$] hydroxide cluster, **2**, with potassium *tert*-butoxide (KOtBu; Scheme 1). The resulting compound, **5**, was crystallographically characterized (Figure 2B); deprotonation of the hydroxide ligand leads to structural changes to the apical Fe in **5**. The Fe4–O2 distance contracts to 1.817(2) Å, compared to the distances in **1** (1.937(1) Å) and the precursor **2** (1.907(3) Å); this bond length matches closely with the structurally characterized Fe^{III}-oxo complexes reported by Borovik and Fout.[8e, 8h, 8i] Compound **6**, prepared by deprotonating **3**, also displays a short Fe4–O2 distance (1.795(8) Å). Furthermore, the apical Fe-μ_4-O distance (Fe4–O1) elongates to 1.965(2) Å in **5** and 2.049(7) Å in **6**, from 1.890(3) Å in **2** and 1.948(2) Å in **3**, which is consistent with a greater trans influence exerted by the terminal oxo ligand. The Mössbauer spectra of **5** and **6** are consistent with the [$Fe^{III}_2Fe^{II}_2$] and [$Fe^{III}_3Fe^{II}$] oxidation state assignments, respectively (Figure 2D and S54). The quadrupole doublet assigned to the apical Fe^{III}-oxo centers in **5** and **6** have parameters distinct from the other previously reported data for **$[(H_3beau)Fe(O)]^{2-}$**, and most other terminal Fe-oxo complexes (Table 1).[8e, 12] Further spectroscopic studies of these Fe^{III}-oxo clusters are underway to understand the source of their atypical Mössbauer parameters.

Terminal Fe^{III}-oxo complexes are rare, and typically stabilized through hydrogen bonding interactions.[8e, 8h, 8i, 13] The structures of **5** and **6** display comparable hydrogen bonding distances to other structurally characterized Fe^{III}-oxo complexes, **$[(H_3beau)Fe(O)]^{2-}$** and **$[N(afa^{Cy})_3Fe(O)]^{+}$**, along with similar equatorial Fe–N distances (Table 1). However, the μ_4-O distances in **5** (1.965(2) Å) and **6** (2.049(7) Å) are significantly shorter than the Fe–N

distances for the amine trans to the oxo in the mononuclear systems (~2.27 Å). This is likely a result of greater ligand flexibility in the mononuclear systems; the geometry of these Fe^{III}-oxo complexes display greater deviations from ideal trigonal bipyramidal geometry compared to the apical Fe in **5** and **6**, based on a structural index parameter (τ; ideal trigonal bipyramidal geometry = 1.0). For the clusters reported here, the rigid geometry of the pyrazolate ligands prevents significant distortion of the apical Fe out of the equatorial plane.

The hydroxide ligand in **2** was determined to be very basic in THF (pK_a = 30.1; Table S1). Analogous equilibrium studies were performed on **3** and, as expected, oxidation of the cluster reduces the basicity of the Fe^{III}-oxo moiety (pK_a = 23.0 for **3**; Table S2). Attempts to deprotonate **4** with various bases, even at low temperatures, only resulted in decomposition, so a pK_a value for this oxidation state was not measured. These data were combined with electrochemical information for clusters 1 (vide supra) and 5 (Figure S38), to produce thermodynamic square schemes according to equation 1 (Figure 3):[14]

$$\mathrm{BDE_{O-H}} = 23.06\,E^{\circ} + 1.37\mathrm{p}K_a + C \quad (1)$$

Similar to our previously reported studies on [Fe_3Mn] hydroxide and aquo clusters, the bond dissociation enthalpy of the O–H bond ($BDE_{O–H}$) increases upon oxidation of the distal Fe centers, ranging from 72 kcal/mol in **1** to 84 kcal/mol in **3**.[15]

The three distal Fe oxidation states have a dramatic effect on the reactivity of the Fe^{III}-oxo center through modifying the pK_a and $BDE_{O–H}$ values. For example, **5** is incapable of performing proton coupled electron transfer (PCET) reactions[16,17] with substituted phenols over a range of phenol $BDE_{O–H}$ values (79 – 85 kcal/mol); only proton transfer to generate **2** is observed as expected from the combination of low $BDE_{O–H}$ for **1** and high pK_a of **2** (Figure 3, Table 2 and Figure S13). Oxidation of the remote Fe centers in **6** and **7** enables PCET reactivity with these phenols (Figures S14 and S16), resulting in the formation of **2** and **3**, respectively.

^{31}P NMR and GC/MS analyses suggest that **7** is capable of transferring an oxygen atom to trimethylphoshine (PMe_3), where the other Fe^{III}-oxo clusters display no reaction towards the phosphine on similar timescale (see SI). The difference in reactivity is likely due to the low reduction potentials of **5** and **6** precluding efficient oxygen atom transfer reactivity. A more oxidizing cluster, through oxidations of the distal Fe centers, **7** can undergo OAT.

The kinetics of C–H activation by these clusters was investigated. The reaction between **5** and 9,10-dihydroanthracene (DHA; $BDE_{C–H}$ = 78 kcal/mol)[14c] displays an expected first order dependence on substrate concentration, with an overall second order rate constant of 87 M^{-1} s^{-1}, and a considerable kinetic isotope effect (KIE) of 7 with d_4-DHA. These data are consistent with a rate-limiting C–H bond activation for the PCET process to form **1** and anthracene. The second-order rate constants between **5** and C–H bonds of varying $BDE_{C–H}$ and pK_a values were measured and display a linear dependence of the PCET reaction rate on the pK_a of the organic substrate (Figure 4), suggesting either a concerted or stepwise pK_a-driven process.[18] Reactions between DHA and **6** or **7** produce the corresponding hydroxide-clusters and anthracene in yields comparable to **5** (Table S3) indicating PCET processes, but

complex kinetics precluded the determination of rate constants and further insights into the mechanism of these reactions.

Overall, this report offers a rare systematic study of the effects of neighboring redox active metals on structural and reactivity aspects of a terminal metal-oxo. Because it is part of a cluster, the reactivity of the terminal metal-oxo motif can be tuned without changing the formal redox state of the metal supporting it; however, redox events at distal centers have significant effect on the acidity and BDE of the corresponding O-H bond. Clearly, the cluster as an assembly is essential for reactivity beyond the structural aspects of the isolated metal-oxo motif. Further development of multinuclear model systems is necessary to fully understand the nature and amplitude of these effects.

Supplementary Material

Refer to Web version on PubMed Central for supplementary material.

ACKNOWLEDGMENT

This research was supported by the NIH (R01-GM102687B) and the Dreyfus Teacher-Scholar Program (T.A.). C.J.R. thanks the Resnick Sustainability Institute at Caltech for a fellowship. We thank Dr. Mike Takase and Larry Henling for assistance with crystallography, Prof. Jonas Peters for use of his group's Mössbauer spectrometer, and the Dow Next Generation Educator Fund for instrumentation.

REFERENCES

1. (a)Que L Jr; Tolman WB, Biologically inspired oxidation catalysis. Nature 2008, 455, 333; [PubMed: 18800132] (b)Hohenberger J; Ray K; Meyer K, The biology and chemistry of high-valent iron–oxo and iron–nitrido complexes. Nature Communications 2012, 3, 720;(c)Costas M; Mehn MP; Jensen MP; Que L, Dioxygen activation at mononuclear nonheme iron active sites: enzymes, models, and intermediates. Chem. Rev 2004, 104 (2), 939–986; [PubMed: 14871146] (d)Blakemore JD; Crabtree RH; Brudvig GW, Molecular catalysts for water oxidation. Chem. Rev 2015, 115 (23), 12974–13005; [PubMed: 26151088] (e)Nguyen AI; Ziegler MS; Oña-Burgos P; Sturzbecher-Hohne M; Kim W; Bellone DE; Tilley TD, Mechanistic investigations of water oxidation by a molecular cobalt oxide analogue: evidence for a highly oxidized intermediate and exclusive terminal oxo participation. J. Am. Chem. Soc 2015, 137 (40), 12865–12872; [PubMed: 26390993] (f)Okamura M; Kondo M; Kuga R; Kurashige Y; Yanai T; Hayami S; Praneeth VKK; Yoshida M; Yoneda K; Kawata S; Masaoka S, A pentanuclear iron catalyst designed for water oxidation. Nature 2016, 530 (7591), 465–468; [PubMed: 26863188] (g)Hunter BM; Thompson NB; Müller AM; Rossman GR; Hill MG; Winkler JR; Gray HB, Trapping an iron(VI) water-splitting intermediate in nonaqueous media. Joule 2018, 2 (4), 747–763.
2. Yano J; Yachandra V, Mn_4Ca cluster in photosynthesis: where and how water is oxidized to dioxygen. Chem. Rev 2014, 114 (8), 4175–4205. [PubMed: 24684576]
3. (a)Ichino T; Yoshioka Y, Theoretical study on mechanism of dioxygen evolution in photosystem II. II. Molecular and electronic structures at the S_3 and S_4 states of oxygen-evolving complex. Chem. Phys. Lett 2014, 595–596, 237–241;(b)Yamaguchi K; Isobe H; Yamanaka S; Saito T; Kanda K; Shoji M; Umena Y; Kawakami K; Shen JR; Kamiya N; Okumura M, Full geometry optimizations of the mixed-valence $CaMn_4O_4X(H_2O)_4$ (X=OH or O) cluster in OEC of PS II: Degree of symmetry breaking of the labile Mn-X-Mn bond revealed by several hybrid DFT calculations. Int. J. Quantum Chem 2013, 113 (4), 525–541;(c)Sproviero EM; Gascón JA; McEvoy JP; Brudvig GW; Batista VS, Quantum mechanics/molecular mechanics study of the catalytic cycle of water splitting in photosystem II. J. Am. Chem. Soc 2008, 130 (11), 3428–3442; [PubMed: 18290643] (d)Siegbahn, P. E. M., Water oxidation mechanism in photosystem II, including oxidations, proton release pathways, O—O bond formation and O_2 release. BBA - Bioenergetics 2013, 1827 (8), 1003–1019. [PubMed: 23103385]

4. Limburg J; Vrettos JS; Liable-Sands LM; Rheingold AL; Crabtree RH; Brudvig GW, A functional model for O-O bond formation by the O_2-evolving complex in photosystem II. Science 1999, 283 (5407), 1524–1527. [PubMed: 10066173]
5. (a)Ozaki S.-i.; Roach MP; Matsui T; Watanabe Y, Investigations of the roles of the distal heme environment and the proximal heme iron ligand in peroxide activation by heme enzymes via molecular engineering of myoglobin. Acc. Chem. Res 2001, 34 (10), 818–825; [PubMed: 11601966] (b)Betley TA; Wu Q; Van Voorhis T; Nocera DG, Electronic design criteria for O−O bond formation via metal−oxo complexes. Inorg. Chem 2008, 47 (6), 1849–1861; [PubMed: 18330975] (c)Guo M; Corona T; Ray K; Nam W, Heme and Nonheme High-Valent Iron and Manganese Oxo Cores in Biological and Abiological Oxidation Reactions. ACS Cent Sci 2019, 5 (1), 13–28; [PubMed: 30693322] (d)Sacramento JJD; Goldberg DP, Factors affecting hydrogen atom transfer reactivity of metal–oxo porphyrinoid complexes. Acc. Chem. Res 2018, 51 (11), 2641–2652; [PubMed: 30403479] (e)Goetz MK; Hill EA; Filatov AS; Anderson JS, Isolation of a terminal Co(III)-oxo complex. J. Am. Chem. Soc 2018, 140 (41), 13176–13180; [PubMed: 30078327] (f)Usharani D; Janardanan D; Li C; Shaik S, A theory for bioinorganic chemical reactivity of oxometal complexes and analogous oxidants: the exchange and orbital-selection rules. Acc. Chem. Res 2013, 46 (2), 471–482; [PubMed: 23210564] (g)Kim SH; Park H; Seo MS; Kubo M; Ogura T; Klajn J; Gryko DT; Valentine JS; Nam W, Reversible O−O bond cleavage and formation between Mn(IV)-peroxo and Mn(V)-oxo corroles. J. Am. Chem. Soc 2010, 132 (40), 14030–14032; [PubMed: 20845972] (h)Kurahashi T; Kikuchi A; Shiro Y; Hada M; Fujii H, Unique properties and reactivity of high-valent manganese-oxo versus manganese-hydroxo in the salen platform. Inorg. Chem 2010, 49 (14), 6664–6672; [PubMed: 20553024] (i)Gunay A; Theopold KH, C−H bond activations by metal oxo compounds. Chem. Rev 2010, 110 (2), 1060–1081. [PubMed: 20143877]
6. (a)de Visser SP; Kumar D; Neumann R; Shaik S, Computer-generated high-valent iron–oxo and manganese–oxo species with polyoxometalate ligands: how do they compare with the iron–oxo active species of heme enzymes? Angew. Chem. Int. Ed 2004, 43 (42), 5661–5665;(b)Khenkin AM; Kumar D; Shaik S; Neumann R, Characterization of manganese(V)−oxo polyoxometalate intermediates and their properties in oxygen-transfer reactions. J. Am. Chem. Soc 2006, 128 (48), 15451–15460; [PubMed: 17132012] (c)Xue G; De Hont R; Münck E; Que L Jr., Million-fold activation of the $[Fe_2(\mu\text{-}O)_2]$ diamond core for C-H bond cleavage. Nature Chemistry 2010, 2 (5), 400–405;(d)Vaddypally S; Kondaveeti SK; Karki S; Van Vliet MM; Levis RJ; Zdilla MJ, Reactive pendant Mn=O in a synthetic structural model of a proposed S_4 state in the photosynthetic oxygen evolving complex. J. Am. Chem. Soc 2017, 139 (13), 4675–4681; [PubMed: 28288514] (e)Sarma R; Angeles-Boza AM; Brinkley DW; Roth JP, Studies of the di-iron(VI) intermediate in ferrate-dependent oxygen evolution from water. J. Am. Chem. Soc 2012, 134 (37), 15371–15386. [PubMed: 22900971]
7. (a)Carsch KM; de Ruiter G; Agapie T, Intramolecular C–H and C–F bond oxygenation by site-differentiated tetranuclear manganese models of the OEC. Inorg. Chem 2017, 56 (15), 9044–9054; [PubMed: 28731687] (b)de Ruiter G; Thompson NB; Takase MK; Agapie T, Intramolecular C–H and C–F bond oxygenation mediated by a putative terminal oxo species in tetranuclear iron complexes. J. Am. Chem. Soc 2016, 138 (5), 1486–1489; [PubMed: 26760217] (c)de Ruiter G; Carsch KM; Gul S; Chatterjee R; Thompson NB; Takase MK; Yano J; Agapie T, Accelerated oxygen atom transfer and C−H bond oxygenation by remote redox changes in Fe3Mn-iodosobenzene adducts. Angew. Chem. Int. Ed 2017, 56 (17), 4772–4776.
8. (a)Lacy DC; Gupta R; Stone KL; Greaves J; Ziller JW; Hendrich MP; Borovik AS, Formation, structure, and EPR detection of a high spin Fe^{IV}—oxo species derived from either an Fe^{III}—oxo or Fe^{III}—OH complex. J. Am. Chem. Soc 2010, 132 (35), 12188–12190; [PubMed: 20704272] (b)Gupta R; Taguchi T; Lassalle-Kaiser B; Bominaar EL; Yano J; Hendrich MP; Borovik AS, High-spin Mn–oxo complexes and their relevance to the oxygen-evolving complex within photosystem II. Proc. Natl. Acad. Sci 2015, 112 (17), 5319–5324; [PubMed: 25852147] (c)Gupta R; MacBeth CE; Young VG; Borovik AS, Isolation of monomeric $Mn^{III/II}$–OH and Mn^{III}–O complexes from water: evaluation of O−H bond dissociation energies. J. Am. Chem. Soc 2002, 124 (7), 1136–1137; [PubMed: 11841259] (d)Gupta R; Borovik AS, Monomeric $Mn^{III/II}$ and $Fe^{III/II}$ complexes with terminal hydroxo and oxo ligands: probing reactivity via O−H bond dissociation energies. J. Am. Chem. Soc 2003, 125 (43), 13234–13242; [PubMed: 14570499] (e)MacBeth CE; Golombek AP; Young VG; Yang C; Kuczera K; Hendrich MP; Borovik AS, O_2 activation by nonheme iron

complexes: a monomeric Fe(III)-oxo complex derived from O_2. Science 2000, 289 (5481), 938–941; [PubMed: 10937994] (f)Ford CL; Park YJ; Matson EM; Gordon Z; Fout AR, A bioinspired iron catalyst for nitrate and perchlorate reduction. Science 2016, 354 (6313), 741; [PubMed: 27846604] (g)Park YJ; Matson EM; Nilges MJ; Fout AR, Exploring Mn-O bonding in the context of an electronically flexible secondary coordination sphere: synthesis of a Mn(III)-oxo. Chem. Commun 2015, 51 (25), 5310–5313;(h)Matson EM; Park YJ; Fout AR, Facile nitrite reduction in a non-heme iron system: formation of an iron(III)-Oxo. J. Am. Chem. Soc 2014, 136 (50), 17398–17401; [PubMed: 25470029] (i)Gordon Z; Drummond MJ; Matson EM; Bogart JA; Schelter EJ; Lord RL; Fout AR, Tuning the Fe(II/III) redox potential in nonheme Fe(II)–hydroxo complexes through primary and secondary coordination sphere modifications. Inorg. Chem 2017, 56 (9), 4852–4863. [PubMed: 28394119]

9. Han Z; Horak KT; Lee HB; Agapie T, Tetranuclear manganese models of the OEC displaying hydrogen bonding interactions: application to electrocatalytic water oxidation to hydrogen peroxide. J. Am. Chem. Soc 2017, 139 (27), 9108–9111. [PubMed: 28587453]
10. de Ruiter G; Thompson NB; Lionetti D; Agapie T, Nitric oxide activation by distal redox modulation in tetranuclear iron nitrosyl complexes. J. Am. Chem. Soc 2015, 137 (44), 14094–14106. [PubMed: 26390375]
11. Arnett CH; Chalkley MJ; Agapie T, A thermodynamic model for redox-dependent binding of carbon monoxide at site-differentiated, high spin iron clusters. J. Am. Chem. Soc 2018, 140 (16), 5569–5578. [PubMed: 29589921]
12. McDonald AR; Que L Jr, High-valent nonheme iron-oxo complexes: synthesis, structure, and spectroscopy. Coord. Chem. Rev 2013, 257 (2), 414–428.
13. Andris E; Navrátil R; Jašík J; Puri M; Costas M; Que L; Roithová J, Trapping iron(III)–oxo species at the boundary of the “Oxo Wall”: insights into the nature of the Fe(III)–O bond. J. Am. Chem. Soc 2018, 140 (43), 14391–14400. [PubMed: 30336001]
14. (a)Bordwell FG; Satish AV; Zhang S; Zhang XM, Using thermodynamic cycles to study reactive intermediates. In Pure Appl. Chem, 1995; Vol. 67, p 735;(b)Mayer JM, Hydrogen Atom Abstraction by Metal-Oxo Complexes: Understanding the Analogy with Organic Radical Reactions. Acc. Chem. Res 1998, 31 (8), 441–450;(c)Warren JJ; Tronic TA; Mayer JM, Thermochemistry of proton-coupled electron transfer reagents and its implications. Chem. Rev 2010, 110 (12), 6961–7001. [PubMed: 20925411]
15. Reed CJ; Agapie T, Thermodynamics of proton and electron transfer in tetranuclear clusters with Mn–OH_2/OH motifs relevant to H_2O activation by the oxygen evolving complex in photosystem II. J. Am. Chem. Soc 2018, 140 (34), 10900–10908. [PubMed: 30064207]
16. PCET is broadly referred to here as the transfer of a proton and an electron to different parts of a complex (see ref. 17); the precise mechanism, whether concerted (CPET or EPT) or stepwise (either PTET or ETPT), is left ambiguous, as the present experiments cannot differentiate them..
17. Weinberg DR; Gagliardi CJ; Hull JF; Murphy CF; Kent CA; Westlake BC; Paul A; Ess DH; McCafferty DG; Meyer TJ, Proton-Coupled Electron Transfer. Chem. Rev 2012, 112 (7), 4016–4093. [PubMed: 22702235]
18. Goetz MK; Anderson JS, Experimental Evidence for p Ka-Driven Asynchronicity in C-H Activation by a Terminal Co(III)-Oxo Complex. J. Am. Chem. Soc 2019, 141 (9), 4051–4062. [PubMed: 30739450]

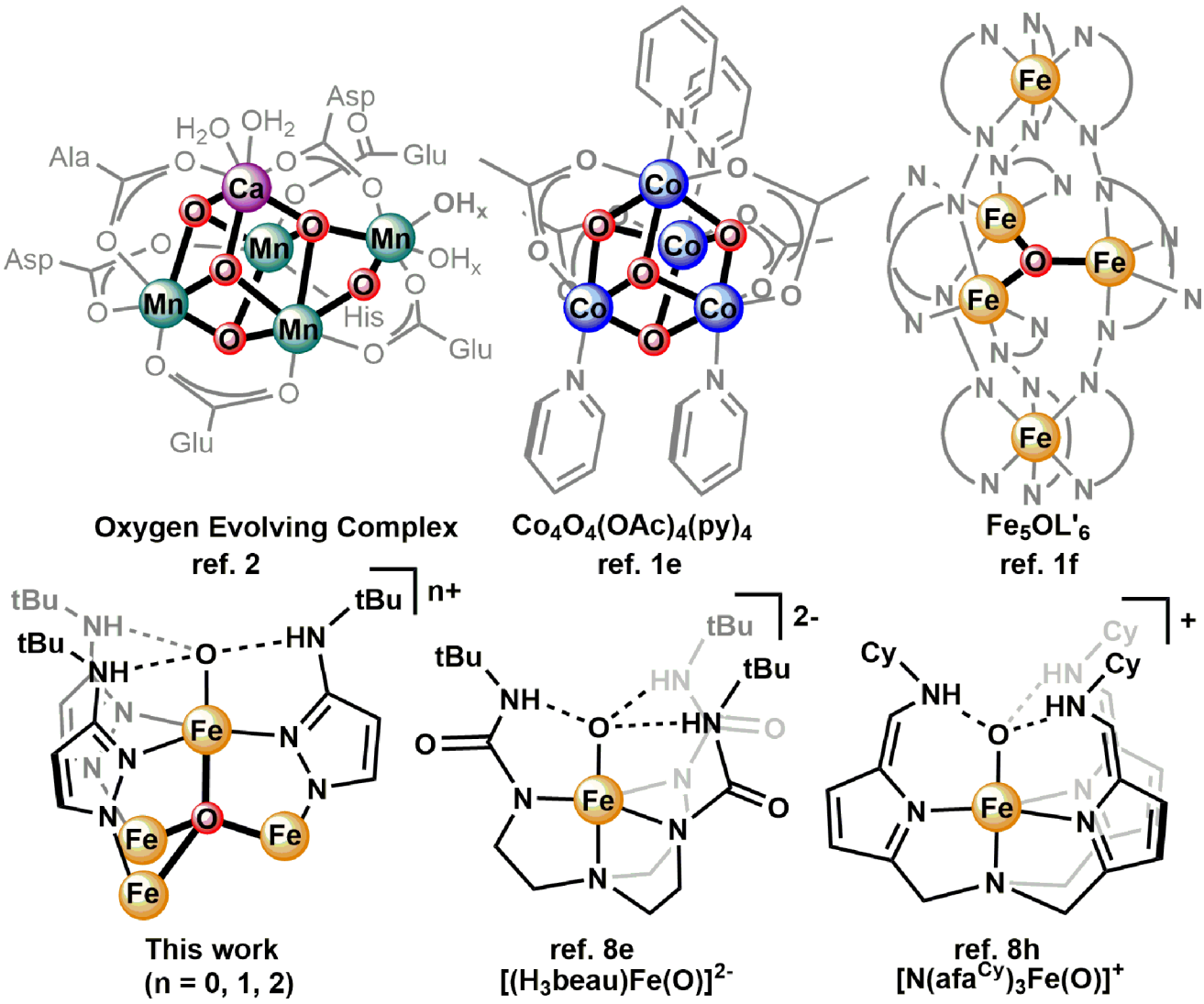

Figure 1.

Multinuclear catalysts with proposed terminal metal-oxo intermediates (top), and structurally characterized terminal Fe^{III}-oxo complexes (bottom)

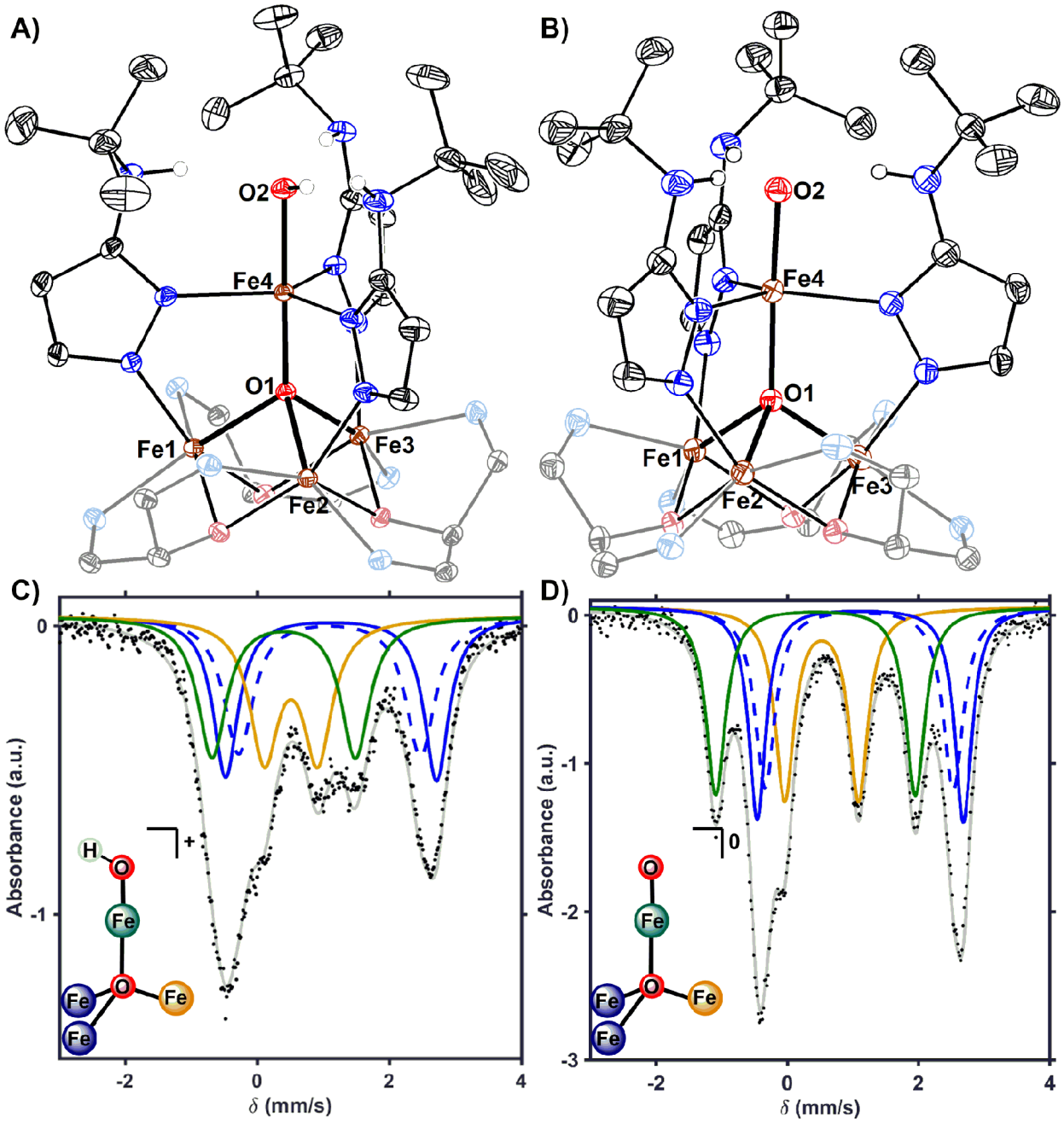

Figure 2.

Crystal structures of tetranuclear Fe hydroxide cluster, **1** (A), and oxo cluster, **5** (B). Ellipsoids shown at the 50% probability level with solvent molecules, and hydrogen atoms (except for N–H moieties) omitted for clarity. (C) Mössbauer spectrum of **2** (black dots) with simulated parameters: (i) δ = 1.12 mm/s, $|\Delta E_q|$ = 3.20 mm/s (solid blue), (ii) δ = 1.10 mm/s, $|\Delta E_q|$ = 2.76 mm/s (dashed blue), (iii) δ = 0.52 mm/s, $|\Delta E_q|$ = 0.81 mm/s (orange), (iv) δ = 0.41 mm/s, $|\Delta E_q|$ = 2.17 mm/s (green). (D) Mössbauer spectrum of **5** (black dots) with simulated parameters: (i) δ = 1.12 mm/s, $|\Delta E_q|$ = 3.14 mm/s (solid blue), (ii) δ = 1.10 mm/s, |

$\Delta E_q| = 2.87$ mm/s (dashed blue), (iii) $\delta = 0.52$ mm/s, $|\Delta E_q| = 1.13$ mm/s (orange), (iv) $\delta = 0.43$ mm/s, $|\Delta E_q| = 3.04$ mm/s (green).

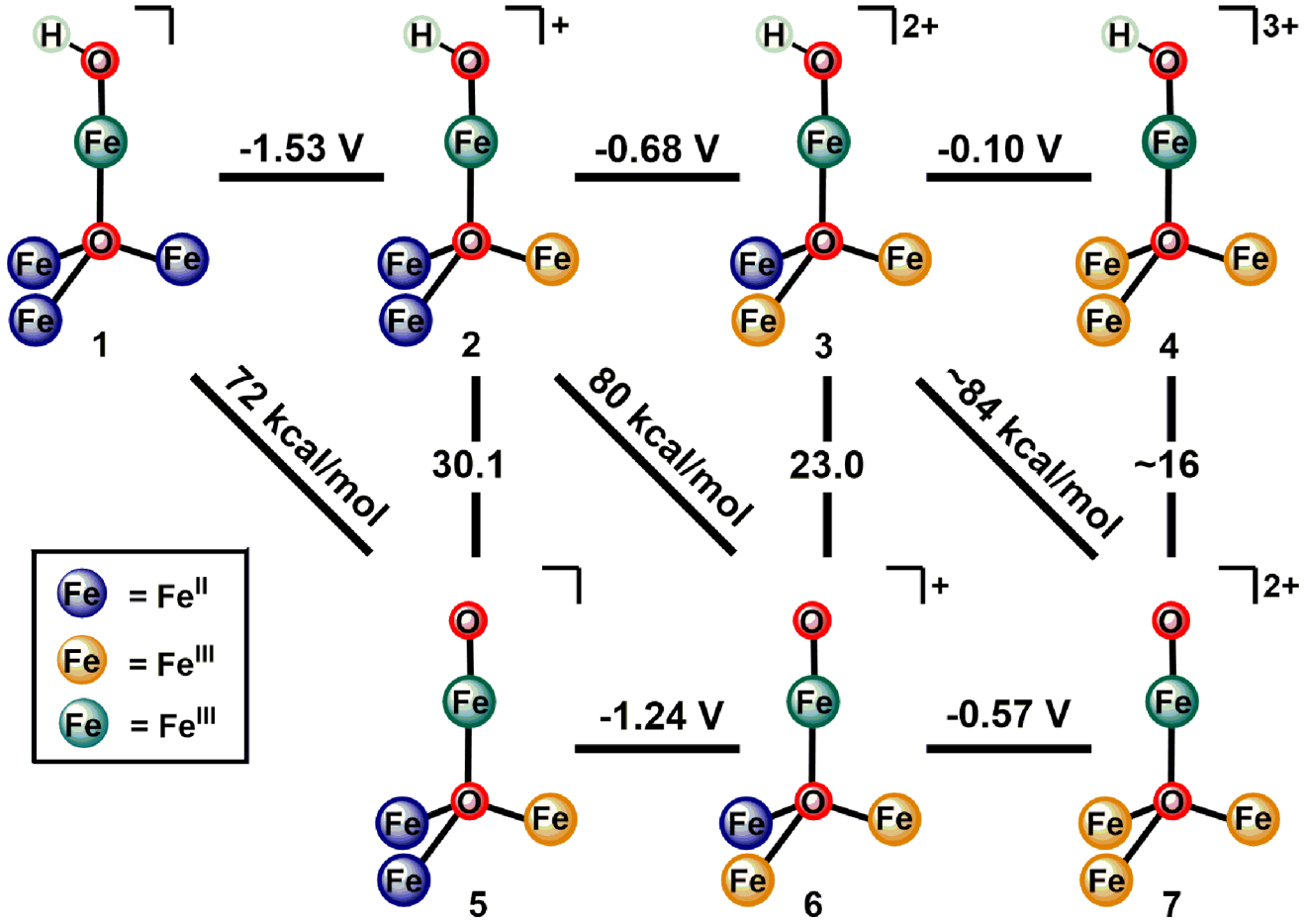

Figure 3.

Thermodynamic cycles to evaluate the $BDE_{O–H}$ values of the hydroxide clusters **1** – **3**. Reduction potentials (horizontal lines) are references to Fc/Fc^+. pK_a values (vertical lines) are based on relative pK_a values of cationic acids in THF. Diagonal lines are the $BDE_{O–H}$ values calculated from these parameters according to the Bordwell equation (eq 1). Approximate values (~) have been extrapolated from the Bordwell equation.

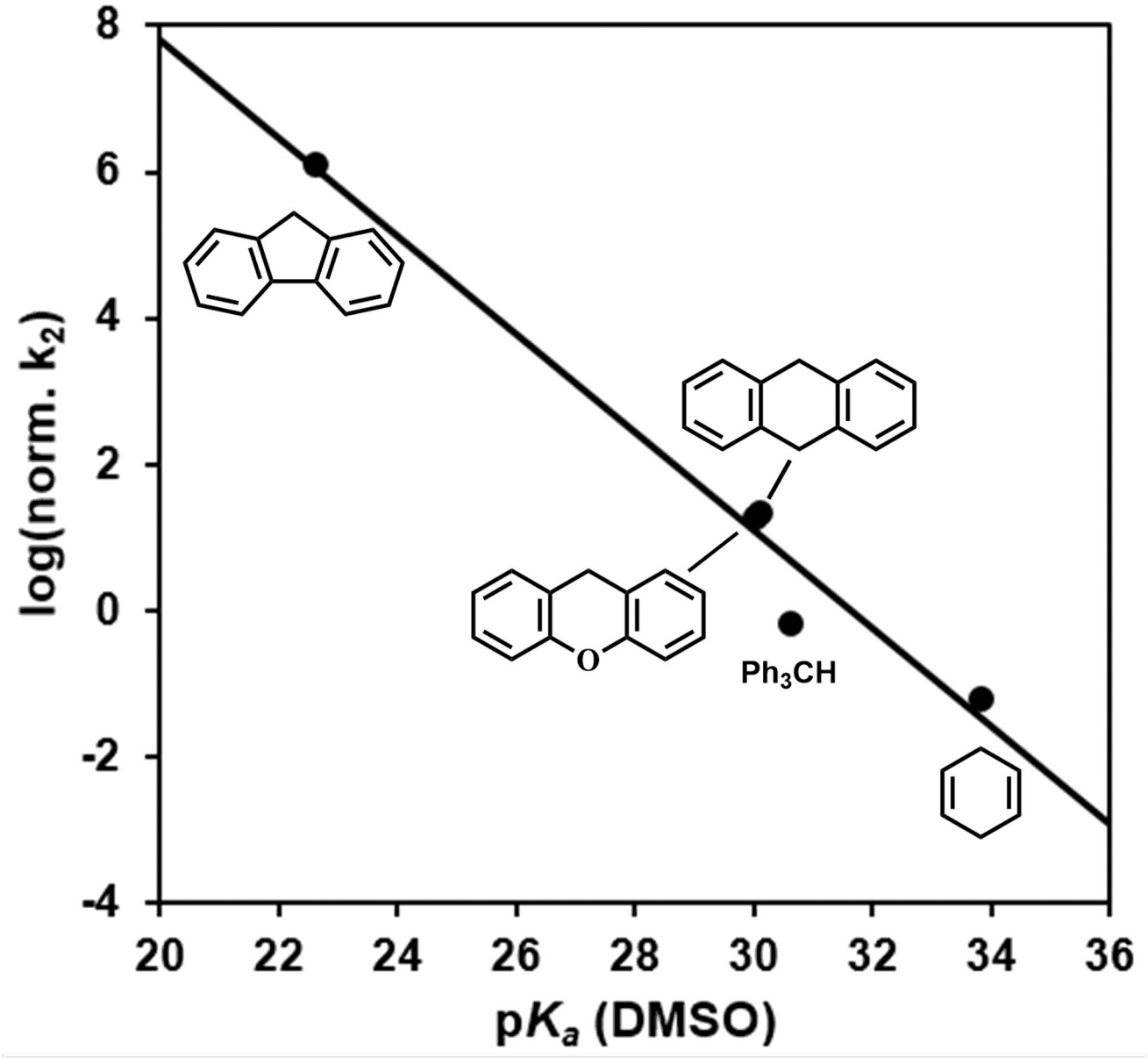

Figure 4.

Plot of log k_2 (normalized to number of reactive C-H bonds) versus reported pK_a values of the organic substrates in DMSO for PCET reactions with **5**.

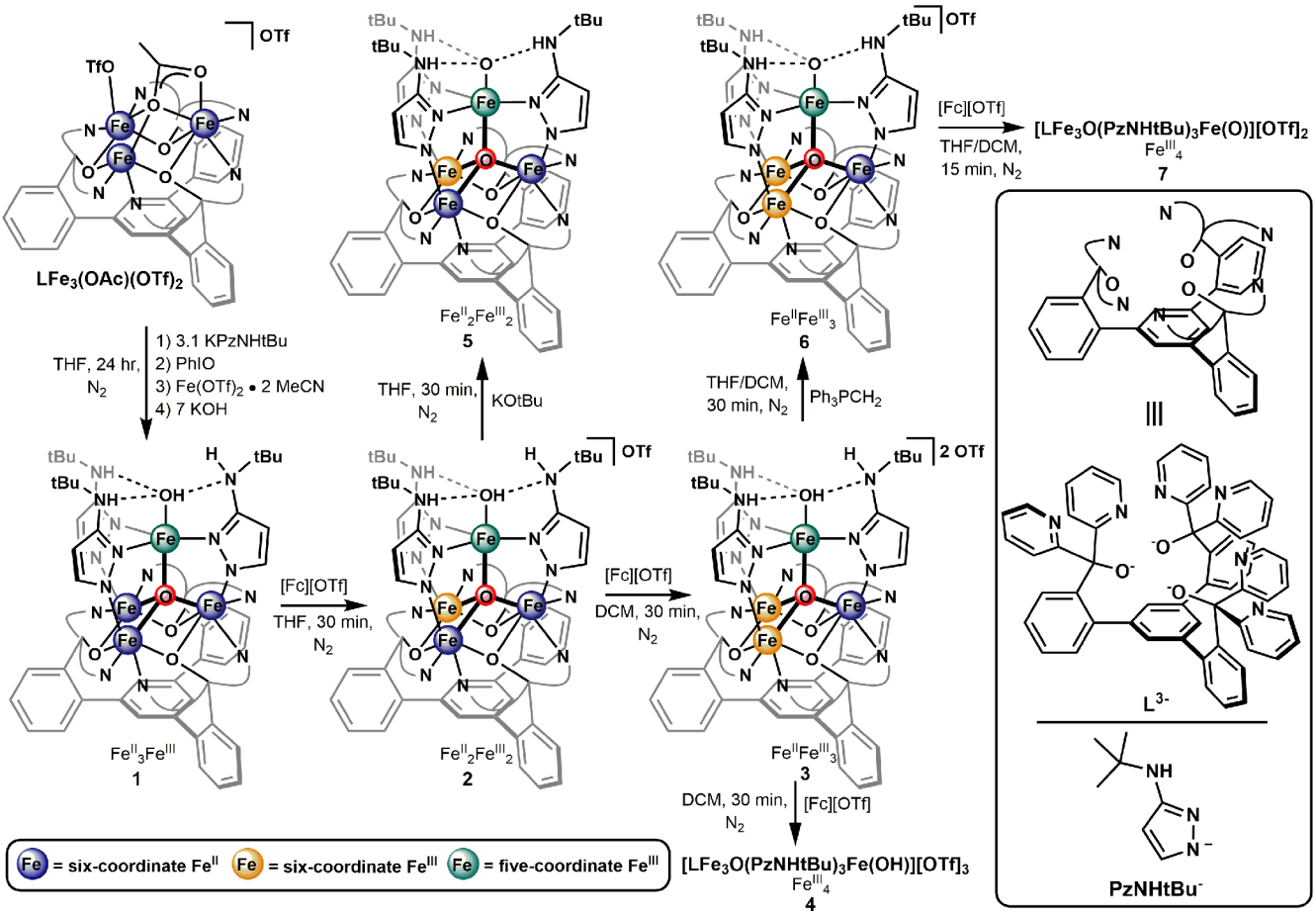

Scheme 1.

Synthesis of [Fe_4] clusters. (Inset) 1,3,5-triarylbenzene ligand platform (L^{3-}) and *tert*-butyl amino pyrazolate ligand ($PzNHtBu^{-}$).

Table 1.

Selected Bond Distances and Angles, Structural Index Parameter, and Mössbauer Parameters of Reported Fe^{III}-Oxo Complexes

	5	**6**	**$[(H_3beau)Fe(O)]^{2-}$** [8e]	**$[N(afa^{Cy})_3Fe(O)]^{+}$** [8h]
Fe–O (Å)	1.817(2)	1.795(8)	1.813(3)	1.806(1)
$Fe–N_{equatorial}$ (Å)	2.104(2), 2.098(2), 2.093(2)	2.100(8), 2.085(9), 2.087(9)	2.030(4), 2.060(4), 2.082(4)	2.049(1), 2.049(1), 2.052(1)
$Fe–L_{trans}$ (Å)	1.965(2) (L=O^{2-})	2.049(7) (L=O^{2-})	2.271(4) (L=NR_3)	2.276(1) (L=NR_3)
N–O (H-bond; Å)	2.647, 2.717, 2.685	2.718, 2.790, 2.750	2.732, 2.702, 2.686	2.641, 2.645, 2.673
$\angle N_{equatorial}$–Fe–O (°)	96.3, 92.8, 92.0	93.6, 97.5, 96.3	103.3, 99.7, 100.8	102.6, 103.1, 103.1
$Fe–N\|N'\|N''_{equatorial}$ (Å)	0.14	0.22	0.42	0.45
Structural Index Parameter (τ)[a]	0.9	0.8	0.5	0.4
Mossbauer parameters (mm/s)	δ = 0.43, $\|\Delta E_q\|$ = 3.04	δ = 0.47, $\|\Delta E_q\|$ = 2.53	δ = 0.30, $\|\Delta E_q\|$ = 0.91	-

[a] $\tau = [\Sigma (\angle N_{equit.}–Fe–N'_{equit.}) - \Sigma (\angle N_{equit.}–Fe–O)]/90$

Table 2.

Reactivity of the [Fe_4]-Oxo Clusters, 5 – 7.

	BDE (kcal/mol)	Reactivity Observed[a]		
		5 ($Fe^{II}_2Fe^{III}_2$)	**6 ($Fe^{II}Fe^{III}_3$)**	**7 (Fe^{III}_4)**
9,10-dihydroanthracene	78	PCET	PCET	PCET
fluorene	82	PCET	PCET	PCET
2,4,6-tBu_3-PhOH	82	PT	PCET	PCET
PMe_3	-	NR	NR	OAT

[a] PT = proton transfer, PCET = proton-coupled electron transfer (based on cluster products), OAT = oxygen atom transfer, NR = no reaction observed.

[b] Second-order rate constant.